Fault Tolerant Homopolar Magnetic Bearings

Ming-hsiu Li, Alan Palazzolo, and Andrew Kenny
Texas A&M University, College Station, Texas

Andrew Provenza, Raymond Beach, and Albert Kascak
Glenn Research Center, Cleveland, Ohio

The NASA STI Program Office . . . in Profile

Since its founding, NASA has been dedicated to the advancement of aeronautics and space science. The NASA Scientific and Technical Information (STI) Program Office plays a key part in helping NASA maintain this important role.

The NASA STI Program Office is operated by Langley Research Center, the Lead Center for NASA's scientific and technical information. The NASA STI Program Office provides access to the NASA STI Database, the largest collection of aeronautical and space science STI in the world. The Program Office is also NASA's institutional mechanism for disseminating the results of its research and development activities. These results are published by NASA in the NASA STI Report Series, which includes the following report types:

- TECHNICAL PUBLICATION. Reports of completed research or a major significant phase of research that present the results of NASA programs and include extensive data or theoretical analysis. Includes compilations of significant scientific and technical data and information deemed to be of continuing reference value. NASA's counterpart of peer-reviewed formal professional papers but has less stringent limitations on manuscript length and extent of graphic presentations.

- TECHNICAL MEMORANDUM. Scientific and technical findings that are preliminary or of specialized interest, e.g., quick release reports, working papers, and bibliographies that contain minimal annotation. Does not contain extensive analysis.

- CONTRACTOR REPORT. Scientific and technical findings by NASA-sponsored contractors and grantees.

- CONFERENCE PUBLICATION. Collected papers from scientific and technical conferences, symposia, seminars, or other meetings sponsored or cosponsored by NASA.

- SPECIAL PUBLICATION. Scientific, technical, or historical information from NASA programs, projects, and missions, often concerned with subjects having substantial public interest.

- TECHNICAL TRANSLATION. English-language translations of foreign scientific and technical material pertinent to NASA's mission.

Specialized services that complement the STI Program Office's diverse offerings include creating custom thesauri, building customized databases, organizing and publishing research results . . . even providing videos.

For more information about the NASA STI Program Office, see the following:

- Access the NASA STI Program Home Page at *http://www.sti.nasa.gov*

- E-mail your question via the Internet to help@sti.nasa.gov

- Fax your question to the NASA Access Help Desk at 301–621–0134

- Telephone the NASA Access Help Desk at 301–621–0390

- Write to:
  NASA Access Help Desk
  NASA Center for AeroSpace Information
  7121 Standard Drive
  Hanover, MD 21076

Fault Tolerant Homopolar Magnetic Bearings

Ming-hsiu Li, Alan Palazzolo, and Andrew Kenny
Texas A&M University, College Station, Texas

Andrew Provenza, Raymond Beach, and Albert Kascak
Glenn Research Center, Cleveland, Ohio

National Aeronautics and
Space Administration

Glenn Research Center

September 2003

Acknowledgments

FAULT TOLERANT HOMOPOLAR MAGNETIC BEARINGS

Ming-hsiu Li, Alan Palazzolo, and Andrew Kenny
Texas A&M University
College Station, Texas 77843

Andrew Provenza, Raymond Beach, and Albert Kascak
National Aeronautics and Space Administration
Glenn Research Center
Cleveland, Ohio 44135

ABSTRACT

Magnetic suspensions (MS) satisfy the long life and low loss conditions demanded by satellite and ISS based flywheels used for Energy Storage and Attitude Control (ACESE) service. This paper summarizes the development of a novel MS that improves reliability via fault tolerant operation. Specifically, flux coupling between poles of a homopolar magnetic bearing is shown to deliver desired forces even after termination of coil currents to a subset of "failed poles". Linear, coordinate decoupled force–voltage relations are also maintained before and after failure by bias linearization. Current distribution matrices (CDM) which adjust the currents and fluxes following a pole set failure are determined for many faulted pole combinations. The CDM's and the system responses are obtained utilizing 1D magnetic circuit models with fringe and leakage factors derived from detailed, 3D, finite element field models. Reliability results are presented vs. detection/correction delay time and individual power amplifier reliability for 4, 6, and 7 pole configurations. Reliability is shown for two "success" criteria, i.e. (a) no catcher bearing contact following pole failures and (b) re-levitation off of the catcher bearings following pole failures. An advantage of the method presented over other redundant operation approaches is a significantly reduced requirement for backup hardware such as additional actuators or power amplifiers.

INTRODUCTION

Attractive magnetic bearing actuators as shown in Fig. 1 possess individual pole forces that vary quadratically with current. The net force of the bearing may be linearized with respect to the control voltages by utilizing a bias flux component.[1,2] Thus the x_1, x_2 and x_3 forces become decoupled, i.e. dependent only on their respective control voltages (V_{c1}, V_{c2}, V_{c3}). Maslen and Meeker[3] provided a generalization of this approach for heteropolar magnetic bearings (HEMB), which derive their bias flux from electric coils and utilize both N and S at different poles.

Fault tolerant control of HEMB's has been demonstrated on a 5 axis, flexible rotor test rig with 3 CPU failures and 2 (out of 8) adjacent coil failures.[4] Current distribution matrices for HEMB's were extended to cover 5 pole failures out of 8 poles[5,6] and for the case of significant effects of material path reluctance and fringing.[7]

The fault tolerant approach outlined above utilizes a current distribution matrix (CDM) that changes the current in each pole after failure in order to achieve linearized, decoupled relations between control forces and control voltages, i.e.

$$f_{cj} = K_{vj} V_{cj} \qquad j = 1,2,3 \qquad (1)$$

A failure configuration is defined by the subset of poles that fail due either to shorting of a turn in a coil or to failure of a power amplifier. In general there exist $(2^n - 1)$ number of possible failure configurations for an n pole magnetic bearing.

A unique contribution of the present work includes the extension of a CDM approach to 4, 6 and 7 pole homopolar magnetic bearings (HOMB). The HOMB commonly uses permanent magnets for its bias flux to increase the actuator's efficiency and reduce heat generation.[8] Points on the surface of the spinning journal in the homopolar bearing do not experience north-south flux reversals thereby reducing rotor losses due to hysteresis and eddy currents.

A second contribution of the present work is an investigation of the reliabilities of fault-tolerant HOMB. The reliabilities presented are system specific for two reasons.

(a) An exact solution CDM may not exist for certain pole failure configurations. An approximate solution will always exist though and its effectiveness is verified or nullified via failure simulation for the specific system studied.

(b) The two types of reliability presented correspond to whether a successful outcome is defined by:

Successful outcome 1 (SO1): No contact between the shaft and catcher bearings during the failure and CDM implementation sequence, or

Successful outcome 2 (SO2): Shaft contact with a catcher bearing then re-levitation occurs during the failure and CDM implementation sequence.

Satisfaction of these success criteria will depend on the system studied and the delay time τ_d required to identify which poles have failed, to turn off the power amplifiers for these poles and to implement the corresponding CDM for the remaining poles.

Two types of successful outcomes are defined in order to provide the system designer with magnetic bearing component reliabilities estimates which are either independent (SO1) or dependent (SO2) on the accuracy of the catcher bearing simulation model. Therefore reliabilities are presented for the SO1 and SO2 conditions and for a range of τ_d values.

The specific system employed for this study is a high speed flywheel under development for energy storage and attitude control applications on satellites or on the ISS (International Space Station). A general result identified from the study is an increase in reliability as the number of poles increase.

FAULT TOLERANT CONTROL (FTC) REQUIREMENTS

Derivation of the FTC approach requires applications of Ampere's, Ohm's, Faraday's Laws and the Maxwell Stress Tensor to the multi-path magnetic circuit in a magnetic bearing. The physical requirements of FTC include

(1) Decoupling Condition: The x_i control voltage (V_{c_i}) does not affect the x_j control force (F_{x_j}) unless i = j, where $x_1 = x$ (radial) $x_2 = y$ (radial) and $x_3 = z$ (axial).

$$\frac{\partial F_{x_j}}{\partial V_{c_i}} = 0, \ i \neq j \text{ and } i, j = 1,2,3 \qquad (2)$$

(2) Linearity Condition: The x_i control voltage (V_{c_i}) and x_i control force (F_{x_i}) are linearly related.

$$F_{x_i} = K_{v_i} V_{c_i}, \qquad i = 1,2,3 \qquad (3)$$

where K_{v_i} is evaluated at the desired operating location of the shaft in the bearing.

(3) Invariance Condition 1: The gains K_{v_i} are not affected by the failure.

(4) Invariance Condition 2: The force/position gains

$$K_{p_i} = \frac{\partial F_{x_i}}{\partial x_i}\bigg|_{V_{cj}=0, X_j = X_{j0},(j=1,2,3)}, \qquad i = 1,2,3 \qquad (4)$$

are not affected by the failure. The steady state operating point of the shaft in the bearing has coordinates x_{j0}.

The FTC requirement, Eq. (4), is automatically satisfied for a magnetic bearing with bias fluxes generated by permanent magnets (PM). This results since the PM's and the resulting bias flux are unaffected by the failure state of the poles.

A complete derivation of the FTC theory is developed next for a 6 pole homopolar combination (combo, radial and axial forces) magnetic bearing (6PHCB). The FTC theory for the 4 and 7 pole bearings is very similar and is not included.

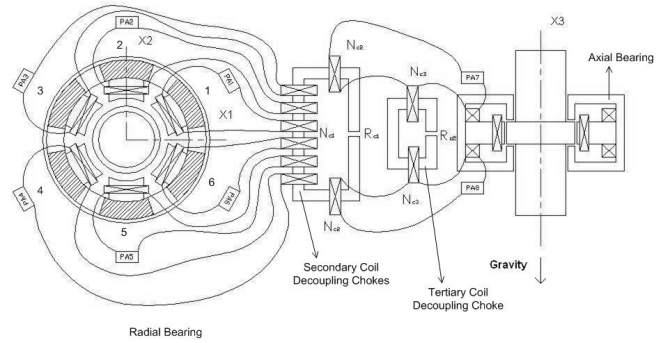### Six (6) Pole Homopolar Combo Bearing (6PHCB)

Fig. 1 Six Pole Homopolar Combo Bearing

Figure 1 depicts a combination (radial/axial) 6PHCB installed on a vertically directed shaft. The actuator has 6 radial poles and coils and 2 axial poles and coils. The axial coils are wound circumferentially around the shaft and the radial coils are wound around the poles. The coil leads also form secondary coils around a common de-coupling choke (DC) and the axial leads also form tertiary coils around a second DC. The DC's eliminate mutual inductances and insure that the inductance matrix is non-singular, which insures electric circuit stability.[2] The laminated construction provides for an accurate approximation of infinite bandwidth between currents and fluxes. Following common practice, the actuator is modeled as an equivalent circuit with derated magnetic strength accounting for leakage and derated gap flux density (B_i) to account for fringing. Figure 2 shows the 6 flux paths through the radial poles and 2 flux paths through the axial poles.
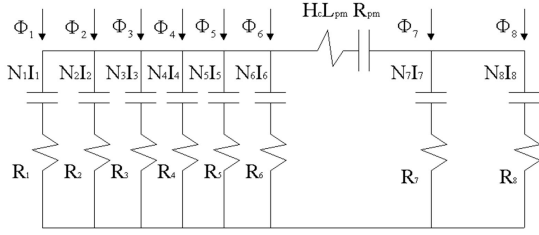
Fig. 2 Equivalent Magnetic Circuit for the Six Pole Homopolar Combo Bearing

The NI sources represent radial and axial control current flux sources. The $H_c L_{pm}$ and R_{pm} terms represent the permanent magnet source strength for driving bias flux, Φ_B, and the reluctance of the permanent magnet, respectively. The magnetic circuit provides a useful tool to present flux conservation and Ampere Law relations with an equivalent electric circuit model. Kirchhoff's law applied to Fig. 2 yields.

$$\begin{bmatrix} R_1 & -R_2 & 0 & 0 & 0 & 0 & 0 & 0 \\ 0 & R_2 & -R_3 & 0 & 0 & 0 & 0 & 0 \\ 0 & 0 & R_3 & -R_4 & 0 & 0 & 0 & 0 \\ 0 & 0 & 0 & R_4 & -R_5 & 0 & 0 & 0 \\ 0 & 0 & 0 & 0 & R_5 & -R_6 & 0 & 0 \\ R_{pm} & R_{pm} & R_{pm} & R_{pm} & R_{pm} & R_{pm}+R_6 & -R_7 & 0 \\ 0 & 0 & 0 & 0 & 0 & 0 & R_7 & -R_8 \\ 1 & 1 & 1 & 1 & 1 & 1 & 1 & 1 \end{bmatrix} \begin{bmatrix} \Phi_1 \\ \Phi_2 \\ \Phi_3 \\ \Phi_4 \\ \Phi_5 \\ \Phi_6 \\ \Phi_7 \\ \Phi_8 \end{bmatrix} =$$

$$\begin{bmatrix} N_1 & -N_2 & 0 & 0 & 0 & 0 & 0 & 0 \\ 0 & N_2 & -N_3 & 0 & 0 & 0 & 0 & 0 \\ 0 & 0 & N_3 & -N_4 & 0 & 0 & 0 & 0 \\ 0 & 0 & 0 & N_4 & -N_5 & 0 & 0 & 0 \\ 0 & 0 & 0 & 0 & N_5 & -N_6 & 0 & 0 \\ 0 & 0 & 0 & 0 & 0 & N_6 & -N_7 & 0 \\ 0 & 0 & 0 & 0 & 0 & 0 & N_7 & -N_8 \\ 0 & 0 & 0 & 0 & 0 & 0 & 0 & 0 \end{bmatrix} \begin{bmatrix} I_1 \\ I_2 \\ I_3 \\ I_4 \\ I_5 \\ I_6 \\ I_7 \\ I_8 \end{bmatrix} + \begin{bmatrix} 0 \\ 0 \\ 0 \\ 0 \\ 0 \\ H_c L_{pm} \\ 0 \\ 0 \end{bmatrix}$$

$$R\Phi = NI + H \qquad (5)$$

Let A represent a diagonal matrix of pole gap areas then by assuming uniform flux densities in each gap

$$AB = \Phi \qquad (6)$$

$$B = A^{-1}R^{-1}NI + A^{-1}R^{-1}H = VI + B_{bias} \qquad (7)$$

$$V = A^{-1}R^{-1}N \qquad (8)$$

$$B_{bias} = A^{-1}R^{-1}H \qquad (9)$$

where the reluctance of gap i is

$$R_i = g_i / (\mu_0 a_i) \qquad (10)$$

and N_i and a_i are the number of turns on pole i and the gap-cross section area, respectively. The term V in Eq. (8) and the VI term in Eq. (7) show that the control flux (VI) varies with control current and with shaft position (gap values), however the bias flux (B_{bias}) varies solely with shaft position.

Magnetic bearings typically utilize servo power amplifiers (PA) that provide 1.2-2.0 kHz bandwidth for inductive loads ranging between 2 mH to 8 mH. Thus it is acceptable to use a constant for the control current per control voltage gain. Let

$$V_c = (V_{c1} \quad V_{c2} \quad V_{c3})^T \qquad (11)$$

represent the control voltages and the 8×3 matrix T is the current distribution matrix (CDM). Then in the absence of pole failures

$$I' = TV_c \qquad (12)$$

where T includes the PA gain and the current distribution terms.

Fault conditions are represented using the matrix K that has a null row for each faulted pole. Then the failed actuator control currents become

$$I = KI' = KTV_c \qquad (13)$$

For example if coils 1 and 2 fail

$$K = \begin{bmatrix} 0 & 0 & 0 & 0 & 0 & 0 & 0 & 0 \\ 0 & 0 & 0 & 0 & 0 & 0 & 0 & 0 \\ 0 & 0 & 1 & 0 & 0 & 0 & 0 & 0 \\ 0 & 0 & 0 & 1 & 0 & 0 & 0 & 0 \\ 0 & 0 & 0 & 0 & 1 & 0 & 0 & 0 \\ 0 & 0 & 0 & 0 & 0 & 1 & 0 & 0 \\ 0 & 0 & 0 & 0 & 0 & 0 & 1 & 0 \\ 0 & 0 & 0 & 0 & 0 & 0 & 0 & 1 \end{bmatrix} \qquad (14)$$

The magnetic forces are determined from the Maxwell stress tensor as;

$$F_j = B^T \gamma_j B \qquad (15)$$

where

$$\gamma_1 = diag[\frac{a_i \cos\theta_i}{2\mu_0}], i = 1 \sim 6, \ \gamma_1(7,7) = \gamma_1(8,8) = 0 \qquad (16)$$

$$\gamma_2 = diag[\frac{a_i \sin\theta_i}{2\mu_0}], i = 1 \sim 6, \ \gamma_2(7,7) = \gamma_2(8,8) = 0 \qquad (17)$$

$\gamma_3(7,7) = -\gamma_3(8,8) = \dfrac{a'}{2\mu_0}$, all other components are zero

$$(18)$$

Substitute Eq. (13) into Eq. (7):

$$B = VI + B_{bias} = VKTVc + B_{bias} = WVc + B_{bias} \quad (19)$$

where $W = VKT$

The magnetic forces are given in terms of control voltages and bias flux density as;

$$
\begin{aligned}
F_j &= (WVc + B_{bias})^T \gamma_j (WVc + B_{bias}) \\
&= Vc^T W^T \gamma_j WVc + 2B_{bias}^T \gamma_j WVc + B_{bias}^T \gamma_j B_{bias} \\
j &= 1,2,3
\end{aligned}
\quad (20)
$$

The magnetic forces are proportional to the square of control voltages in Eq. (20). The following constraint equations must be satisfied in order to meet FTC requirements 1 (Eq. 2), 2 (Eq. 3), and 3.

$$W^T \gamma_1 W = 0_{3x3} \quad (21)$$

$$2B_{bias}^T \gamma_1 W = \begin{bmatrix} K_{v1} & 0 & 0 \end{bmatrix} \quad (22)$$

$$W^T \gamma_2 W = 0_{3x3} \quad (23)$$

$$2B_{bias}^T \gamma_2 W = \begin{bmatrix} 0 & K_{v2} & 0 \end{bmatrix} \quad (24)$$

$$W^T \gamma_3 W = 0_{3x3} \quad (25)$$

$$2B_{bias}^T \gamma_3 W = \begin{bmatrix} 0 & 0 & K_{v3} \end{bmatrix} \quad (26)$$

Let

$$W = \begin{bmatrix} W_1 & W_2 & W_3 \end{bmatrix} \quad (27)$$

Then the 27 constraint equations become

$$W_i^T \gamma_j W_k = 0, \quad i,j,k = 1,2,3 \text{ and } k \geq i \quad (28)$$

$$B_{bias}^T \gamma_i W_j = \begin{cases} 0 & \text{for } i \neq j \\ K_{vi}/2 & \text{for } i = j \end{cases}, \quad i,j = 1,2,3 \text{ and } j \geq i \quad (29)$$

Equations (28) and (29) are 18 nonlinear and 9 linear algebraic equations for the CDM entries, t_{ij}. The CDM matrix entries are obtained by requiring simultaneous

solution of the equations in Eq. (28) and (29), and minimization of the Frobenius matrix norm of the CDM matrix. This is typically performed at the magnetic center, i.e. the location where the bias flux balances the static loads on the bearing. The norm of the current vector, I in Eq (13), satisfies the consistency condition[9]

$$\|I\| \leq \|K\| \cdot \|T\| \cdot \|V_c\| \quad (30)$$

where for a Frobenius norm

$$\|K\| = \sqrt{\sum_{i,j} K_{ij}^2} \quad (31)$$

$$\|T\| = \sqrt{\sum_{i,j} t_{ij}^2} \quad (32)$$

$$\|V_c\| = \sqrt{\sum_i V_{ci}^2} \quad (33)$$

Thus by Eq. (30) reduction of $\|I\|$ follows from minimizing $\|T\|$. The Lagrange multiplier approach is employed to locate a solution of the equations in Eq. (28) and (29), that minimize $\|T\|$. The cost function is

$$L = \sum_{i=1}^{p} \sum_{j=1}^{3} t_{ij}^2 + \sum_{k=1}^{27} \lambda_k h_k \quad (34)$$

where p is the number of functioning poles and h_k are the constraint equations in Eq. (28) and (29). The solution condition is;

$$\frac{\partial L}{\partial Z_m} = \underline{0}, \quad Z_m \in \{t_{ij}, \lambda_k\} \quad (35)$$

which implies

$$
F(t_{ij}, \lambda_k) = \begin{bmatrix} h_1 & \cdots & h_{27} & \dfrac{\partial L}{\partial t_{11}} & \dfrac{\partial L}{\partial t_{12}} & \dfrac{\partial L}{\partial t_{13}} & \cdots & \dfrac{\partial L}{\partial t_{p1}} & \dfrac{\partial L}{\partial t_{p2}} & \dfrac{\partial L}{\partial t_{p3}} \end{bmatrix}^T
$$
$$= \begin{bmatrix} 0 & \cdots & 0 \end{bmatrix}^T$$

$$(36)$$

The total set of equation is over-determined, i.e. more equations than unknowns, therefore a solution exists only in the least square (LS) sense. The nonlinear equation, LS based solver available in MATLAB is employed for this purpose. The effectiveness of each solution in satisfying the FTC requirements must be checked by transient response simulation of the

respective fault event since the LS solution is not exact. Fortunately the feedback control action compensates for the presence of residuals in the solution of Eq. (35), in many instances.

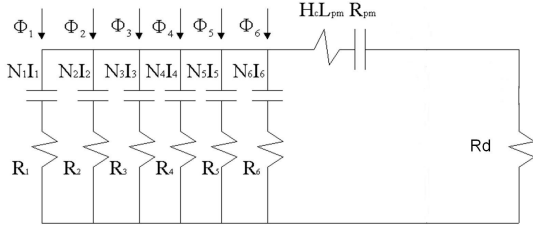## 6 Pole Homopolar Radial Bearing (6PHRB)

Fig. 3 Equivalent Magnetic Circuit for the Six Pole Homopolar Radial Bearing

The 6PHRB provides force solely in the two transverse (radial) directions. A magnetic circuit model for this bearing is illustrated in Fig. 3. The flux-current relations for this circuit are obtained by applying Kirchoff's laws, which yield

$$
\begin{bmatrix}
R_1 & -R_2 & 0 & 0 & 0 & 0 \\
0 & R_2 & -R_3 & 0 & 0 & 0 \\
0 & 0 & R_3 & -R_4 & 0 & 0 \\
0 & 0 & 0 & R_4 & -R_5 & 0 \\
0 & 0 & 0 & 0 & R_5 & -R6 \\
R_d+R_{pm} & R_d+R_{pm} & R_d+R_{pm} & R_d+R_{pm} & R_d+R_{pm} & R_d+R_{pm}+R_6
\end{bmatrix}
\begin{bmatrix}
\Phi_1 \\ \Phi_2 \\ \Phi_3 \\ \Phi_4 \\ \Phi_5 \\ \Phi_6
\end{bmatrix} =
$$

$$
\begin{bmatrix}
N_1 & -N_2 & 0 & 0 & 0 & 0 \\
0 & N_2 & -N_3 & 0 & 0 & 0 \\
0 & 0 & N_3 & -N_4 & 0 & 0 \\
0 & 0 & 0 & N_4 & -N_5 & 0 \\
0 & 0 & 0 & 0 & N_5 & -N_6 \\
0 & 0 & 0 & 0 & 0 & N_6
\end{bmatrix}
\begin{bmatrix}
I_1 \\ I_2 \\ I_3 \\ I_4 \\ I_5 \\ I_6
\end{bmatrix} +
\begin{bmatrix}
0 \\ 0 \\ 0 \\ 0 \\ 0 \\ H_c L_{pm}
\end{bmatrix}
\quad (37)
$$

where

$$
R_d = \frac{1}{\mu_0 a_d} \sqrt{g_{0d}^2 - x_1^2 - x_2^2} \quad (38)
$$

The FTC requirements result in 10 constraint equations

$$
W^T \gamma_1 W = 0_{2x2} \quad (39)
$$

$$
2B_{bias}^T \gamma_1 W = \begin{bmatrix} K_{v1} & 0 \end{bmatrix} \quad (40)
$$

$$
W^T \gamma_2 W = 0_{2x2} \quad (41)
$$

$$
2B_{bias}^T \gamma_2 W = \begin{bmatrix} 0 & K_{v2} \end{bmatrix} \quad (42)
$$

These equations are solved for t_{ij} and λ_k utilizing the Lagrange multiplier/nonlinear least square solver approach discussed for the 6PHCB.

Decoupling Choke

The inductance matrix of the isolated combo bearing is singular because flux conservation introduces a dependency relation between the fluxes. This produces a potentially unstable operation state for the power amplifiers. Two decoupling chokes are added to the combo bearing according to the approach.[2] By adjusting the parameters of the decoupling chokes ($N_{c1}, N_{c2}, N_{c3}, R_{c1}$, and R_{c2}) the inductance matrix becomes full rank and the mutual inductances become zero. Similarly, a single decoupling choke is added to the radial bearing.

Force Linearization

An exact solution for the t_{ij} can be obtained only for the no-poles failed case. Consequently the FTC linearization and decoupling conditions are only approximately satisfied and the force expressions in Eq. (20) are still somewhat nonlinear. Closed loop, coupled, flexible body simulations of the flywheel rim and shaft, housing, gimbals, and support structure provide predictions of stability, transient and steady-state harmonic responses. Efficient run-times for these models require linearized expressions for the x_1, x_2 and x_3 magnetic forces. These expressions are obtained by applying a two-term Taylor series expansion about the operating point $P_0 = \{x_j = x_{j0}, v_{cj} = v_{cj0}\}$. This yields

$$
F_i = \sum_{j=1}^{3} \left\{ -K_{pij}\left(x_j - x_{j0}\right) + K_{vij}\left(v_{cj} - v_{cj0}\right) \right\} \quad (43)
$$

$$
K_{pij} = -\frac{\partial F_i}{\partial x_j}\Big|_{P_0} = -\frac{\partial(B_{bias}^T \gamma_i B_{bias})}{\partial x_j}\Big|_{P_0} = -\left(2B_{bias}^T \gamma_i \frac{\partial B_{bias}}{\partial x_j}\right)\Big|_{P_0} \quad (44)
$$

$$
K_{vij} = \frac{\partial F_i}{\partial v_{cj}}\Big|_{P_0} = \frac{\partial(2B_{bias}^T \gamma_i WVc)}{\partial v_{cj}}\Big|_{P_0} = (2B_{bias}^T \gamma_i W \frac{\partial Vc}{\partial v_{cj}})\Big|_{P_0} \quad (45)
$$

for i=1,2,3 and j=1,2,3. The K_{pij} and K_{vij} expressions in Eq. (44) and Eq. (45) are referred to as "position" and "voltage" stiffnesses respectively. The K_{vij} terms are zero for $i \neq j$, only if Eq. (36) is satisfied exactly. Equation (20) shows that the K_{pij}, as defined in Eq. (44), are independent of the t_{ij}, when V_{co} is a null vector, which is typically true.
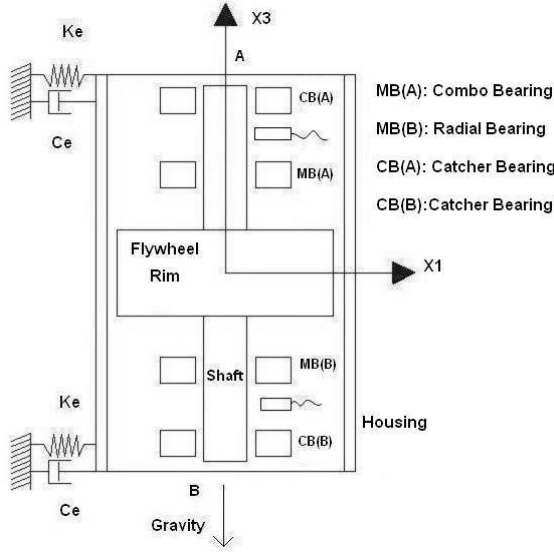
Fig. 4 Flywheel System with a Magnetic Suspension

Flywheel and Magnetic Suspension Dynamics Model

The novel redundant actuators operate within a feedback controlled system that includes both electrical component and structural component dynamics. A typical application is a flywheel module consisting of a high speed shaft, integrally mounted motor-generator, composite flywheel rim, magnetic suspension and flexibly mounted housing. Figure 4 depicts a module model with 9 rigid body structural degrees of freedom: rotor CG translations (X_{1r}, X_{2r}, X_{3r}), rotor rotations (θ_{1r}, θ_{2r}), housing CG translations (X_{1h}, X_{2h}) and housing rotation (θ_{1h}, θ_{2h}). The magnetic suspension employs magnetic (MB) and backup (catcher, CB) bearings at both the A and B ends of the module. Magnetic bearing clearances are approximately 0.5 mm so small angle motion may be assumed. Let b, d and c denote the magnetic actuator (Eq. 20), mass imbalance and catcher bearing forces, respectively. The structural equations of motion for the rotor are:

$$M_r \ddot{X}_{ir} = F_{ib}^A + F_{ib}^B + F_{id}^A + F_{id}^B + F_{ic}^A + F_{ic}^B \quad i=1,2 \quad (46)$$

$$M_r \ddot{X}_{3r} = F_{3b}^A - M_r g + F_{3c}^A \quad (47)$$

$$I_{tr} \ddot{\theta}_{1r} + I_{pr}\omega\dot{\theta}_{2r} = M_{1r} + M_{1rc}^A + M_{1rc}^B \quad (48)$$

$$I_{tr} \ddot{\theta}_{2r} - I_{pr}\omega\dot{\theta}_{1r} = M_{2r} + M_{2rc}^A + M_{2rc}^B \quad (49)$$

For the housing the equations of motion are:

$$M_h \ddot{X}_{ih} = F_{ie}^A + F_{ie}^B - F_{ib}^A - F_{ib}^B - F_{ic}^A - F_{ic}^B \quad i=1,2 \quad (50)$$

$$I_{tih} \ddot{\theta}_{ih} = M_{ih} + M_{ihc}^A + M_{ihc}^B \quad i=1,2 \quad (51)$$

where

$$M_{1r} = -L_{br}^A F_{2b}^A + L_{br}^B F_{2b}^B - L_{dr}^A F_{2d}^A + L_{dr}^B F_{2d}^B \quad (52)$$

$$M_{2r} = L_{br}^A F_{1b}^A - L_{br}^B F_{1b}^B + L_{dr}^A F_{1d}^A - L_{dr}^B F_{1d}^B \quad (53)$$

$$M_{1h} = L_{bh}^A F_{2b}^A - L_{bh}^B F_{2b}^B - L_e^A F_{2e}^A + L_e^B F_{2e}^B \quad (54)$$

$$M_{2h} = -L_{bh}^A F_{1b}^A + L_{bh}^B F_{1b}^B + L_e^A F_{1e}^A - L_e^B F_{1e}^B \quad (55)$$

$$F_{1e}^A = -K_e(X_{1h} + L_e^A \theta_{2h}) - C_e(\dot{X}_{1h} + L_e^A \dot{\theta}_{2h}) \quad (56)$$

$$F_{1e}^B = -K_e(X_{1h} - L_e^B \theta_{2h}) - C_e(\dot{X}_{1h} - L_e^B \dot{\theta}_{2h}) \quad (57)$$

$$F_{2e}^A = -K_e(X_{2h} - L_e^A \theta_{1h}) - C_e(\dot{X}_{2h} - L_e^A \dot{\theta}_{1h}) \quad (58)$$

$$F_{2e}^B = -K_e(X_{2h} + L_e^B \theta_{1h}) - C_e(\dot{X}_{2h} + L_e^B \dot{\theta}_{1h}) \quad (59)$$

The simplified catcher (backup) bearing model shown in Fig. 5 is employed for illustrative purposes in this model. More sophisticated models with internal dynamics of races and balls or rollers are available[10] and could also be used in the system dynamics model.
Let j=1,2 represent the A and B ends of the flywheel module in Fig. 4, respectively. Also let r$_j$ represent the relative displacement between the catcher bearing and shaft at end j.

$$r_j = \sqrt{\left(X_{1rc}^j - X_{1hc}^j\right)^2 + \left(X_{2rc}^j - X_{2hc}^j\right)^2} \quad (60)$$

$$F_n^j = K_c(r_j - r_0) + C_c \dot{r}_j \quad (61)$$

$$F_{1c}^j = -F_n^j(\cos\theta_j - \mu\sin\theta_j) \quad (62)$$

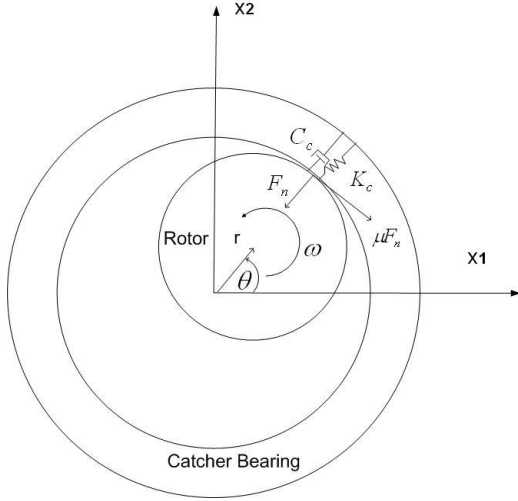$$F_{2c}^j = -F_n^j(\sin\theta_j + \mu\cos\theta_j) \quad (63)$$

Fig. 5 Catcher Bearing Contact Model

Then if r_0 is the catcher bearing clearance and $r_j \geq r_0$

$$M_{1rc}^j = (-1)^j L_{cr}^j F_{2c}^j \tag{64}$$

$$M_{2rc}^j = (-1)^{j+1} L_{cr}^j F_{1c}^j \tag{65}$$

$$M_{1hc}^j = (-1)^{j+1} L_{ch}^j F_{2c}^j \tag{66}$$

$$M_{2hc}^j = (-1)^j L_{ch}^j F_{1c}^j \tag{67}$$

Similarly for the axial direction if $\left|X_{3r}\right| \geq 0$

$$F_{3c}^A = -(K_c (\left|X_{3r}\right| - r_0)\frac{X_{3r}}{\left|X_{3r}\right|} + C_c \dot{X}_{3r}) \tag{68}$$

The mass imbalance disturbance in the model is described by

$$F_{1d}^A = M_r e\omega^2 \cos \omega t \tag{69}$$

$$F_{2d}^A = M_r e\omega^2 \sin \omega t \tag{70}$$

$$F_{1d}^B = M_r e\omega^2 \cos(\omega t + \psi) \tag{71}$$

$$F_{2d}^B = M_r e\omega^2 \sin(\omega t + \psi) \tag{72}$$

The control law utilized in the model is MIMO based and similar to the work of Okada[11] and Ahrens.[12,13] Figure 6 illustrates the overall feedback control loop for the magnetic suspension. Eight power amplifiers are utilized for the combo bearing and 6 power amplifiers for the radial bearing. Five displacement sensors measure the relative displacements between the rotor and housing. Current Distribution matrices (CDM) for the combo and radial bearings are incorporated in the controllers to produce reference voltages for the 14 power amplifiers which produce the desired currents in each coil. The nonlinear magnetic forces are determined according with Eq. (20).
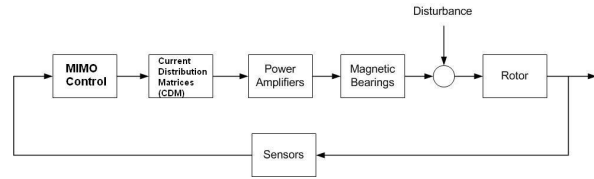

Fig. 6 Magnetic Suspension Control Scheme

EXAMPLES

An example flywheel module illustrates operation and reliability of the redundant magnetic suspension. Table 1 lists the geometrical, inertia and stiffness parameters for the model.

The catcher bearing contact model in Fig. 5 has a stiffness of 10^8 N/m, a damping of 5,000 N-s/m and a dynamic friction coefficient of 0.1. Table 2 shows the magnetic bearing parameters for the MS model.

The 1D magnetic circuit models as shown in Fig. 2 and 3 must be adjusted to include the effects of recirculation leakage of the flux between the N and S poles of any permanent magnet and for the effect of non-parallel (fringing) flux flow in the air gap of each pole. These effects are apparent in a 3D finite element (FE) based simulation of the actuator as shown in Fig. 7. These adjustments are made with multiplicative factors applied to the gap flux and permanent magnetic (PM) coercive force in the 1D model, as derived from the 3D FE model. The PM coercive force is derated from 950,000 to 514,000 in the combo bearing and from 950,000 to 566,000 in the radial bearing. The air gap flux's are derated with a fringe factor of 0.9 for both the combo and radial bearings.
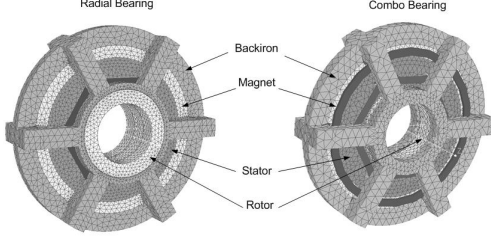
Fig. 7   3D FE Model of the Combo and Radial 6 Pole Actuators

The remaining parameters of the system model include
Displacement Sensor Sensitivity = 7874 V/m
Displacement Sensor Bandwidth = 5000 Hz
 Power Amplifier DC Gain = 1 A/V
Power Amplifier Bandwidth = 1200 Hz
These 3D bearing models were also employed to verify the fault tolerant operation predicted with the 1D model. An example of this is the 3 pole failure results shown in Table 3. The control voltage sets in this table are;

$$V_c = \begin{pmatrix} V_{c1} & V_{c2} & V_{c3} \end{pmatrix}^T = \begin{cases} (1V & 0 & 0)^T & for & set & 1 \\ (0 & 1V & 0)^T & for & set & 2 \\ (0 & 0 & 1V)^T & for & set & 3 \end{cases} \quad (73)$$

The inductance matrix of the combo bearing with the two decoupling chokes is given in henries as;

$$L_{CB} = \begin{bmatrix} 5.59\times10^{-4} & 0 & 0 & 0 & 0 & 0 & 0 & 0 \\ 0 & 5.59\times10^{-4} & 0 & 0 & 0 & 0 & 0 & 0 \\ 0 & 0 & 5.59\times10^{-4} & 0 & 0 & 0 & 0 & 0 \\ 0 & 0 & 0 & 5.59\times10^{-4} & 0 & 0 & 0 & 0 \\ 0 & 0 & 0 & 0 & 5.59\times10^{-4} & 0 & 0 & 0 \\ 0 & 0 & 0 & 0 & 0 & 5.59\times10^{-4} & 0 & 0 \\ 0 & 0 & 0 & 0 & 0 & 0 & 5.83\times10^{-3} & 0 \\ 0 & 0 & 0 & 0 & 0 & 0 & 0 & 5.83\times10^{-3} \end{bmatrix} \quad (74)$$

The inductance matrix of the radial bearing with a decoupling choke is given in henries as;

$$L_{RB} = \begin{bmatrix} 6.76\times10^{-4} & 0 & 0 & 0 & 0 & 0 \\ 0 & 6.76\times10^{-4} & 0 & 0 & 0 & 0 \\ 0 & 0 & 6.76\times10^{-4} & 0 & 0 & 0 \\ 0 & 0 & 0 & 6.76\times10^{-4} & 0 & 0 \\ 0 & 0 & 0 & 0 & 6.76\times10^{-4} & 0 \\ 0 & 0 & 0 & 0 & 0 & 6.76\times10^{-4} \end{bmatrix} \quad (75)$$

The current produced by a power amplifier (PA) is turned off at the moment of failure which simulates an open circuit. This is implemented in the model by changing the K matrix in Eq. (13) from the identity matrix to its pole-failed value, i.e. a null row j for each failed pole j, while the no-pole failed CDM is retained. The appropriate CDM for the pole-failure configuration being tested is then swapped in following a delay time τ_d. The MIMO control law in Fig. 6 is invariant throughout the entire simulation. The combo and radial bearing CDM's for the no pole failed state are

$$T_o^A = \begin{bmatrix} 0.30789 & 0.17776 & 0 \\ 0 & 0.35552 & 0 \\ -0.30789 & 0.17776 & 0 \\ -0.30789 & -0.17776 & 0 \\ 0 & -0.35552 & 0 \\ 0.30789 & -0.17776 & 0 \\ 0 & 0 & -0.11530 \\ 0 & 0 & 0.11530 \end{bmatrix} \quad \text{and}$$

$$T_o^B = \begin{bmatrix} 0.28074 & 0.16209 \\ 0 & 0.32417 \\ -0.28074 & 0.16209 \\ -0.28074 & -0.16209 \\ 0 & -0.32417 \\ 0.28074 & -0.16209 \end{bmatrix} \quad (76)$$

The new CDM's for the poles 1-2-3 failed case in Fig. 1 are

$$T_{123}^A = \begin{bmatrix} 0 & 0 & 0 \\ 0 & 0 & 0 \\ 0 & 0 & 0 \\ -0.61552 & -0.37074 & 0 \\ 0 & -0.69571 & 0 \\ 0.61552 & -0.37074 & 0 \\ 0 & 0 & -0.11530 \\ 0 & 0 & 0.11530 \end{bmatrix} \quad \text{and}$$

$$T_{123}^B = \begin{bmatrix} 0 & 0 \\ 0 & 0 \\ 0 & 0 \\ -0.56126 & -0.33768 \\ 0 & -0.63476 \\ 0.56124 & -0.33768 \end{bmatrix} \quad (77)$$

The new CDM's for the poles 1-2-3-4 failed case in Fig. 1 are

$$T_{1234}^A = \begin{bmatrix} 0 & 0 & 0 \\ 0 & 0 & 0 \\ 0 & 0 & 0 \\ 0 & 0 & 0 \\ -0.60742 & -1.0622 & 0 \\ 1.2224 & -3.6408 \times 10^{-3} & 0 \\ 0 & 0 & -0.11530 \\ 0 & 0 & 0.11530 \end{bmatrix} \quad \text{and}$$

$$T_{1234}^B = \begin{bmatrix} 0 & 0 \\ 0 & 0 \\ 0 & 0 \\ 0 & 0 \\ -0.55379 & -0.96848 \\ 1.11460 & -3.3556 \times 10^{-3} \end{bmatrix} \quad (78)$$

The text below discusses two illustrative examples that assume identical failures in both the radial and combo bearings. Although this represents an extremely rare occurrence it serves to illustrate the method and analysis presented. Example 1 considers failing radial poles 1, 2 and 3, and example 2 considers failing radial poles 1, 2, 3 and 4 in Fig. 1. Figure 8 reveals that for example 1 excellent control is maintained utilizing the no-poles failed CDM's throughout the entire simulation. Consequently successful outcome criteria SO1 is satisfied independent of the delay time τ_d. The currents in the 6 amplifiers are shown in Fig. 9 and 10 for a failure initiation at 0.1 seconds and a delay duration of 20 ms. In contrast, example 2's SO1 is not always satisfied so that the 1-2-3-4 poles failed CDM's (T_{1234}^A, T_{1234}^B) must be activated after delay τ_d. The displacement and current responses for example 2 are shown in Fig. 11, 12 and 13 for $\tau_d = 20$ ms. The reliability for example 2 will be affected by the selection of SO1 or SO2 and the delay time τ_d.

Successful outcome criteria 2 (SO2) requires that the rotor successfully levitates following contact with the catcher bearings (CB). This is highly dependent on whether backward whirl (BW) develops during the contact period. The BW state occurs due to friction at the contact interface between the shaft and CB, which forces the shaft to whirl (precess) in a direction opposite to the spin direction. Figure 14 shows an example of this state with $\mu=0.3$, $C_c=10^5$ N-s/m and $K_c=10^8$ N/m. The BW eccentricity is the CB clearance (typically 0.25 mm) for a rigid rotor, and possibly a

much larger value for a flexible shaft. The whirl frequency typically ranges from 0.4-1.0 times the spin frequency. This creates a potentially large centrifugal force that can damage the CB's or deflect the shaft into the MB's. The BW condition is mitigated by proper design of the flexible damped support, preload, clearance and friction coefficient for the CB's. Re-levitation off of the CB's is very difficult once BW has fully developed. Figure 15 shows the displacements for a successful re-levitation event with poles 1-2-3-4 failed, $\tau_d=100$ ms and $C_c=5000$ N-s/m.
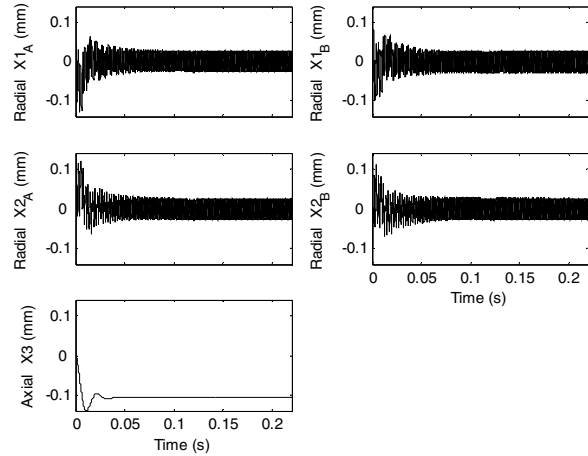

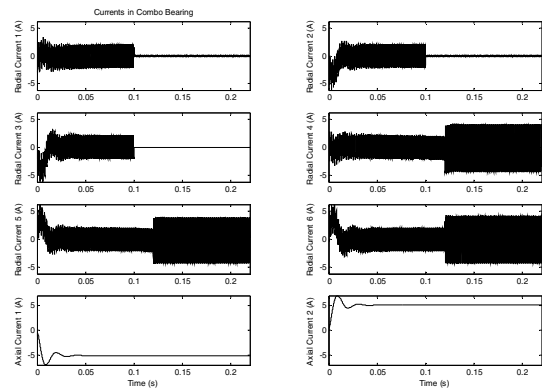Fig. 8 Rotor Displacements in the Radial and Axial Direction for Example 1

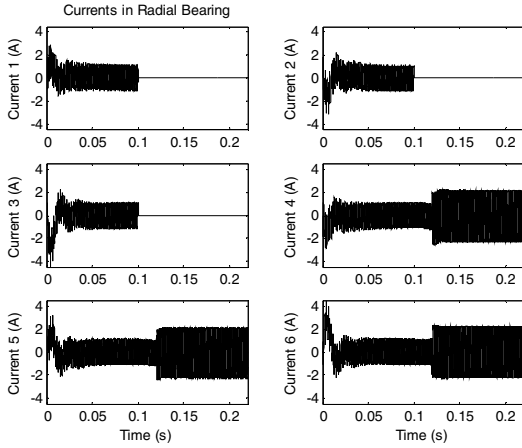Fig. 9 Current Responses in Combo Bearing for Example 1

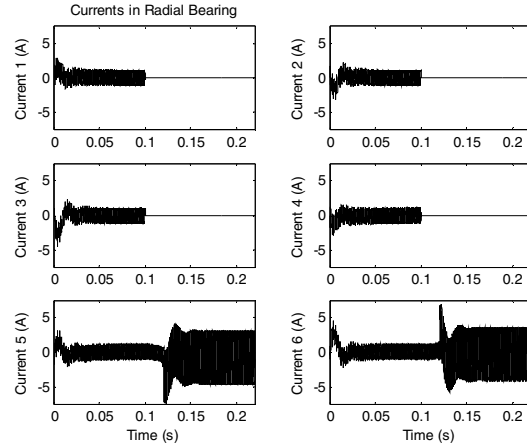Fig. 10 Current Responses in Radial Bearing for
Example 1

Fig. 13 Current Responses in Radial Bearing for
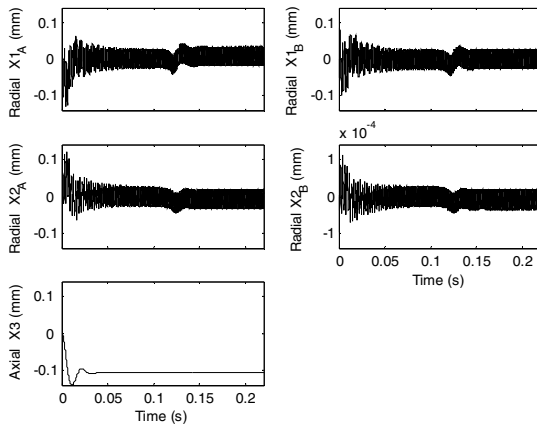Example 2

Fig. 11 Rotor Displacements in the Radial and Axial
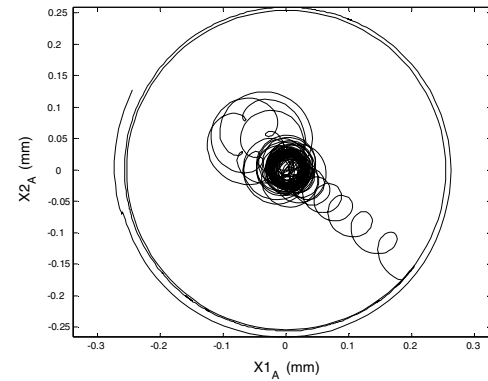Direction for Example 2

Fig. 14 Orbit Plot of the rotor at C.B. 1 with
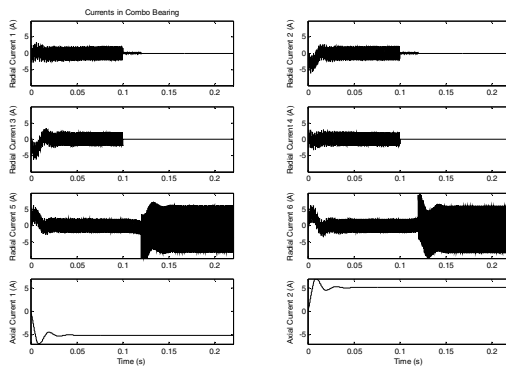$C_c = 10^5$ Nt-m/s

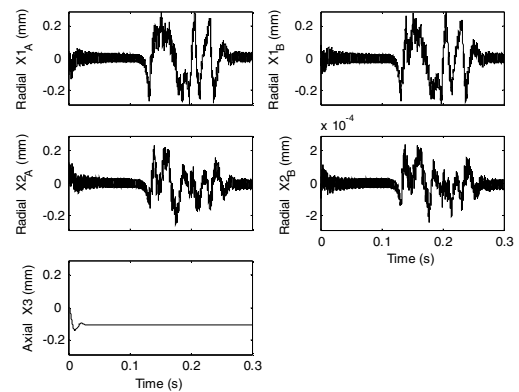Fig. 12 Current Responses in Combo Bearing for
Example 2

Fig. 15 Rotor Displacements in the Radial and Axial
Direction During Successful Re-levitation

The reliability of a magnetic suspension (MS) is determined by considering the number of failed pole states that still meet the SO1 or SO2 criteria. This is dependent on the time delay τ_d, modeling assumptions, number of poles in the bearing and the reliability of the power amplifier/coil units that drive and conduct the bearing currents. The 4 pole and 7 pole configurations require 2 less or 1 more power amplifiers than the 6 pole configuration, respectively. The radial pole and permanent magnet cross-section areas, the number of turns of each radial coil, and the coercive force and the length of the permanent magnets for the 4 and 7 pole bearings are identical to those of the 6 pole bearing.

The no-pole failed CDM's for the 7 pole bearing are

$$
T_o^A = \begin{bmatrix}
0.33071 & -0.017910 & -4.6780\times10^{-3} \\
0.17799 & 0.26601 & 3.6330\times10^{-3} \\
-0.067428 & 0.26396 & -2.7850\times10^{-3} \\
-0.26676 & 0.16181 & 7.8561\times10^{-4} \\
-0.29880 & -0.15575 & 1.7079\times10^{-3} \\
-0.038458 & -0.29204 & -4.2590\times10^{-3} \\
0.15965 & -0.23855 & 4.9591\times10^{-3} \\
0 & 0 & -0.099552 \\
0 & 0 & 0.099552
\end{bmatrix} \quad \text{and}
$$

$$
T_o^B = \begin{bmatrix}
0.28402 & 0 \\
0.17708 & 0.22206 \\
-0.063201 & 0.27690 \\
-0.25589 & 0.12323 \\
-0.25589 & -0.12323 \\
-0.063201 & -0.27690 \\
0.17708 & -0.22206
\end{bmatrix} \quad (79)
$$

The no-pole failed CDM's for the 4 pole bearing are

$$
T_o^A = \begin{bmatrix}
0.52550 & 0 & 0 \\
0 & 0.52550 & 0 \\
-0.52550 & 0 & 0 \\
0 & -0.52550 & 0 \\
0 & 0 & -0.17043 \\
0 & 0 & 0.17043
\end{bmatrix} \quad \text{and}
$$

$$
T_o^B = \begin{bmatrix}
0.46539 & -1.07319\times10^{-3} \\
7.3028\times10^{-4} & 0.46371 \\
-0.46403 & -1.07319\times10^{-3} \\
7.3028\times10^{-4} & -0.46571
\end{bmatrix} \quad (80)
$$

The radial pole failure simulations are conducted with the combo bearing operating in a no-pole failed state, and vice versa. Failure occurs at 0.1 seconds into the simulation and swapping in of the new CDM occurs at a delay time τ_d later. The number of j unfailed pole cases for an n pole bearing is given by the formula

$$
I_{nj} = \binom{n}{j} = \frac{n!}{j!(n-j)!} \quad (81)
$$

Table 4 summarizes the results of these simulations for swapping in the appropriate poles-failed (new) CDM for the delay times τ_d of 20, 60 and 100 ms, respectively. The SO1+SO2 column considers all cases when either SO1 or SO2 occurs.

An n pole, fail-safe, homopolar magnetic bearing is similar to a m-out-of-n system in a reliability model if stable control is maintained (SO1 or SO2) when at minimum m of the n poles (P.A. plus coil) are unfailed. Let R_p represent the reliability of a "pole", i.e. of the power amplifier plus its pole coil, at some specific point in its expected lifetime. Also assume that "poles" are identical and act independently. The system reliability then become

$$
R_S = \sum_{k=m}^{n} \alpha_k R_p^{\ k} (1 - R_p)^{n-k} \quad (82)
$$

where α_k are the number of SO1 (or SO1+SO2) cases in Table 4. The integer m in Eq. (82) is the minimum number of unfailed poles that are required for the n pole bearing to successfully levitate the shaft. The (n,m) pairs determined in this example are (4,2), (6,2) and (7,2). Figures 16-18 show system reliability vs. R_p plots for the 4, 6 and 7 pole radial bearings for SO1 and (SO1+SO2) and τ_d equal to 20, 60 and 100 ms, respectively. Figures 19-21 repeat Fig. 16-18 for the zoomed-in range $0.9 < R_p < 1$. Similarly, Fig. 22-24 show the system reliabilities for radial actuation of the combo bearings. Figure 25-27 repeat Fig. 22-24 for the zoomed-in range $0.9 < R_p < 1$. Axial control reliability is not considered in these figures since it is typically independent of radial direction control.

Table 5 and 6 show system reliabilities R_s for several values of pole reliability R_p. The delay time τ_d, number of poles n, and success criterion are also varied in these tables. A particular notable result shown in these tables is the high reliability of the 4, 6 and 7 pole bearings even if the CDM is not changed after failure.
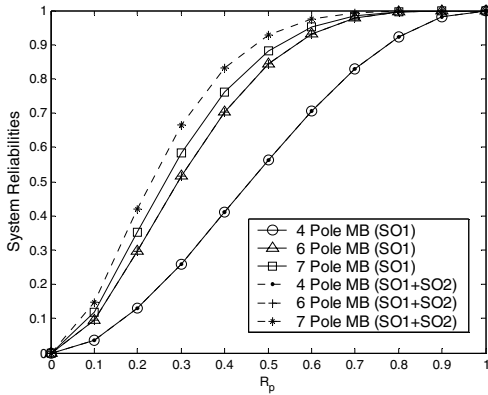
Fig. 16 System Reliabilities of 4, 6 and 7 Pole Radial Bearings with τ_d = 20 ms
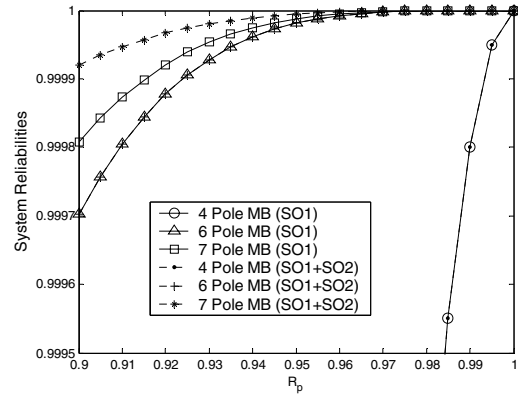

Fig. 19 System Reliabilities of 4, 6 and 7 Pole Radial Bearings with τ_d = 20 ms

Fig. 17 System Reliabilities of 4, 6 and 7 Pole Radial Bearings with τ_d = 60 ms

Fig. 20 System Reliabilities of 4, 6 and 7 Pole Radial Bearings with τ_d = 60 ms
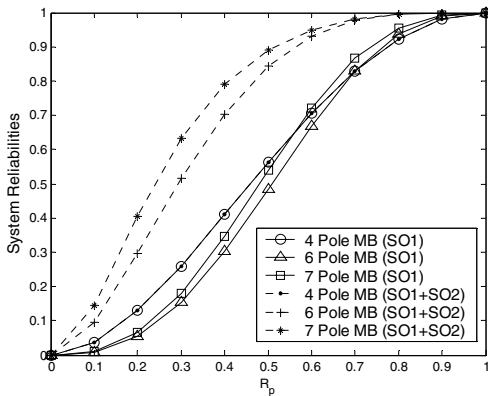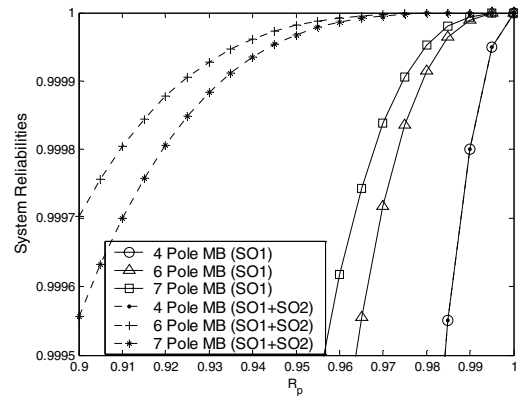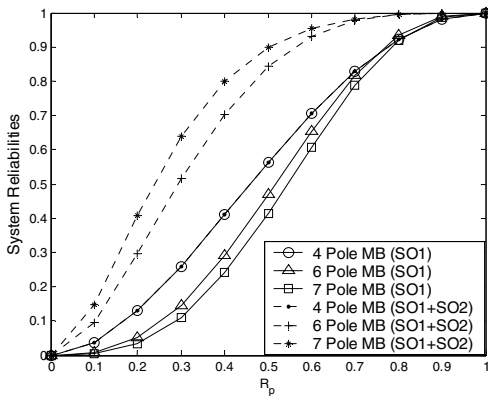

Fig. 18 System Reliabilities of 4, 6 and 7 Pole Radial Bearings with τ_d = 100 ms
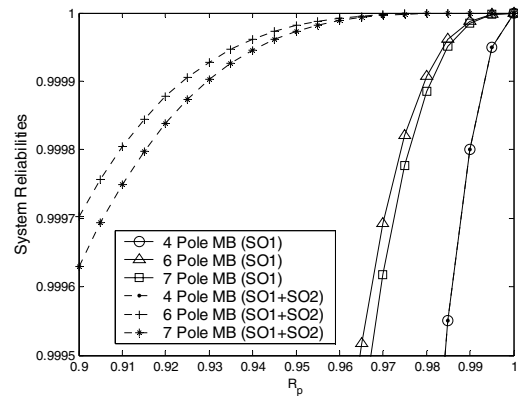

Fig. 21 System Reliabilities of 4, 6 and 7 Pole Radial Bearings with τ_d = 100 ms

Fig. 22 System Reliabilities of 4, 6 and 7 Pole Combo
Bearings with $\tau_d = 20$ ms

Fig. 25 System Reliabilities of 4, 6 and 7 Pole Combo
Bearings with $\tau_d = 20$ ms

Fig. 23 System Reliabilities of 4, 6 and 7 Pole Combo
Bearings with $\tau_d = 60$ ms

Fig. 26 System Reliabilities of 4, 6 and 7 Pole Combo
Bearings with $\tau_d = 60$ ms
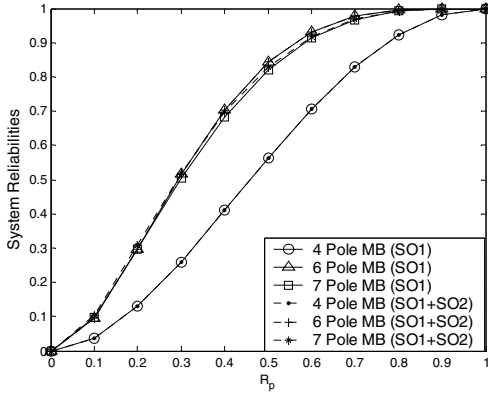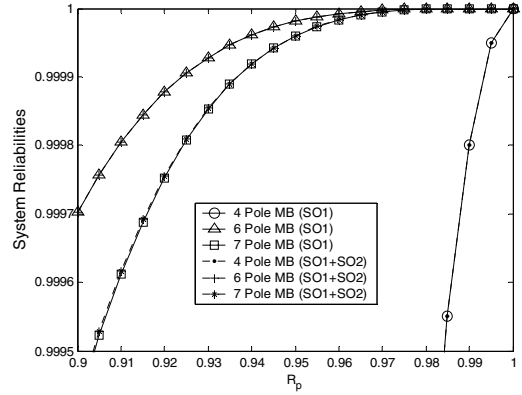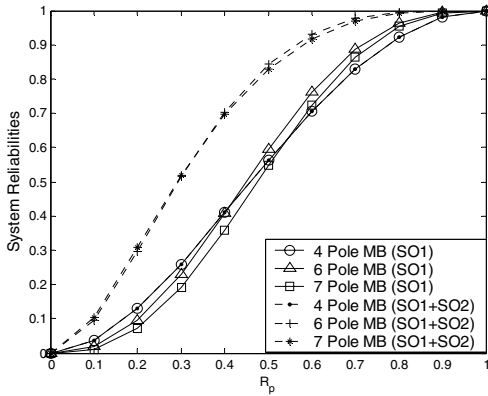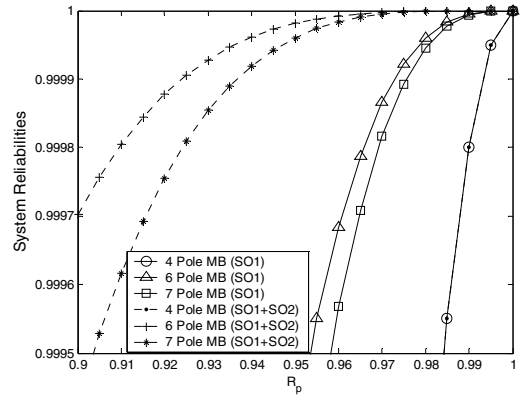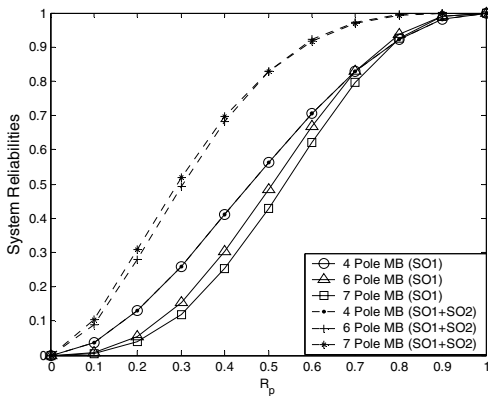

Fig. 24 System Reliabilities of 4, 6 and 7 Pole Combo
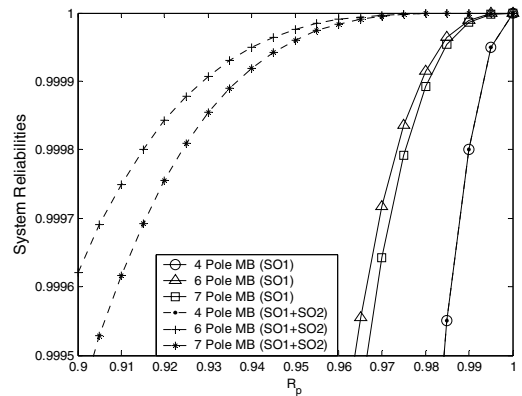Bearings with $\tau_d = 100$ ms

Fig. 27 System Reliabilities of 4, 6 and 7 Pole Combo
Bearings with $\tau_d = 100$ ms

Table 1 Flywheel Model Parameters

M_r	29.644 kg	M_h	34.428 kg
I_{tr}	0.26233 $kg \cdot m^2$	I_{pr}	0.11129 $kg \cdot m^2$
I_{t1h}	1.5337 $kg \cdot m^2$	I_{t2h}	1.3993 $kg \cdot m^2$
K_e	3.5024×10^5 N/m	C_e	5.2535×10^3 kg/s
ω	60,000 rpm	e	2.54×10^{-6} m
L_{br}^A	0.14051 m	L_{br}^B	0.13360 m
L_{dr}^A	0.14051 m	L_{dr}^B	0.13360 m
L_{sr}^A	0.17846 m	L_{sr}^B	0.16974 m
L_{cr}^A	0.26765 m	L_{cr}^B	0.28067 m
L_{bh}^A	0.14051 m	L_{bh}^B	0.13360 m
L_{sh}^A	0.17856 m	L_{sh}^B	0.16974 m
L_{ch}^A	0.26765 m	L_{ch}^B	0.28067 m
L_e^A	0.26765 m	L_e^B	0.28067 m
ψ	$\pi / 2$		

Table 2 Magnetic Bearing Parameter List

	Combo Bearing	Radial Bearing
Air Gap	radial: $5.080 \times 10^{-4} m$ axial: $5.080 \times 10^{-4} m$	radial: $5.080 \times 10^{-4} (m)$ dead pole: $0.00203 (m)$
Radial Pole Face Area	$3.924 \times 10^{-4} (m^2)$	$4.746 \times 10^{-4} (m^2)$
Axial Pole Face Area	$1.719 \times 10^{-3} (m^2)$	N/A
Dead Pole Face Area	N/A	$4.962 \times 10^{-3} (m^2)$
Total Face Area of PM	$3.178 \times 10^{-3} (m^2)$	$3.844 \times 10^{-3} (m^2)$
Length of PM	$0.0101 (m)$	$0.0101 (m)$
Number of Turns of Radial Coil	24	24
Number of Turns of Axial Coil	37	N/A
Relative Permeability of PM	1.055	1.055
Coercive Force of PM	950000 (A/m)	950000 (A/m)

Table 3   1D and 3D Model Comparison of Predicted Forces for 6 Pole Combo Bearing

Control Voltage Set	Force Direction	Force (N)			
		No Poles Failed		3 Poles Failed (Poles 1-2-3	
		1D Model	3D Model	1D Model	3D Model
1	X1	11.64	12.95	11.64	12.96
1	X2	0	0.01	-0.14	-0.25
1	X3	0	0.04	0	-0.03
2	X1	0	0.02	0	-0.08
2	X2	11.64	13.3	11.59	13.17
2	X3	0	0.08	0	-0.05
3	X1	0	-0.4	0	-0.4
3	X2	0	0.66	0	0.66
3	X3	8.9	9.4	8.9	9.4

Table 4 Summary of Simulation for Reliability Study

n pole Bearing	Failed Bearing	No. of unfailed Poles (j)	No. of Simulation (I_{nj})	Delay time τ_d 20 ms		Delay time τ_d 60 ms		Delay time τ_d 100 ms	
				No. of SO1 cases	No. of SO1+SO2 cases	No. of SO1 cases	No. of SO1+SO2 cases	No. of SO1 cases	No. of SO1+SO2 cases
4	Radial	2	6	4	4	4	4	4	4
		3	4	4	4	4	4	4	4
		4	1	1	1	1	1	1	1
	Combo	2	6	4	4	4	4	4	4
		3	4	4	4	4	4	4	4
		4	1	1	1	1	1	1	1
6	Radial	2	15	12	12	0	12	0	12
		3	20	20	20	9	20	8	20
		4	15	15	15	15	15	15	15
		5	6	6	6	6	6	6	6
		6	1	1	1	1	1	1	1
	Combo	2	15	12	12	1	12	0	11
		3	20	20	20	15	20	9	20
		4	15	15	15	15	15	15	15
		5	6	6	6	6	6	6	6
		6	1	1	1	1	1	1	1
7	Radial	2	21	16	21	0	21	0	21
		3	35	33	34	11	29	4	30
		4	35	35	35	29	35	20	35
		5	21	21	21	21	21	21	21
		6	7	7	7	7	7	7	7
		7	1	1	1	1	1	1	1
	Combo	2	21	13	14	0	14	0	14
		3	35	28	28	13	28	5	28
		4	35	35	35	28	35	21	35
		5	21	21	21	21	21	21	21
		6	7	7	7	7	7	7	7
		7	1	1	1	1	1	1	1

Table 5 System Reliabilities of Radial Bearings vs. R_p, n, τ_d and Success Criterion

R_p	τ_d ms	SO1 or SO1+SO2	R_s for CDM Swapped			R_s for No-Poles Failed CDM		
			n=4	n=6	n=7	n=4	n=6	n=7
0.900	20	SO1	0.98010000	0.99970200	0.99980730	0.98010000	0.98998200	0.98772210
	60	SO1	0.98010000	0.99071100	0.99413730			
	100	SO1	0.98010000	0.98998200	0.98772210			
	20	SO1+SO2	0.98010000	0.99970200	0.99992070			
	60	SO1+SO2	0.98010000	0.99970200	0.99955620			
	100	SO1+SO2	0.98010000	0.99970200	0.99962910			
0.950	20	SO1	0.99500625	0.99998128	0.99998777	0.99500625	0.99862753	0.99830066
	60	SO1	0.99500625	0.99873470	0.99925449			
	100	SO1	0.99500625	0.99862753	0.99830066			
	20	SO1+SO2	0.99500625	0.99998128	0.99999454			
	60	SO1+SO2	0.99500625	0.99998128	0.99996774			
	100	SO1+SO2	0.99500625	0.99998128	0.99997310			
0.990	20	SO1	0.99980001	0.99999997	0.99999998	0.99980001	0.99998821	0.99998529
	60	SO1	0.99980001	0.99998918	0.99999400			
	100	SO1	0.99980001	0.99998821	0.99998529			
	20	SO1+SO2	0.99980001	0.99999997	0.99999999			
	60	SO1+SO2	0.99980001	0.99999997	0.99999994			
	100	SO1+SO2	0.99980001	0.99999997	0.99999995			

Table 6 System Reliabilities for Radial Actuation of the Combo Bearings vs. R_p, n, τ_d and Success Criterion

R_p	τ_d ms	SO1 or SO1+SO2	R_s for CDM Swapped			R_s for No-Poles Failed CDM		
			n=4	n=6	n=7	n=4	n=6	n=7
0.900	20	SO1	0.98010000	0.99970200	0.99941850	0.98010000	0.990711	0.98845110
	60	SO1	0.98010000	0.99516600	0.99362700			
	100	SO1	0.98010000	0.99071100	0.98845110			
	20	SO1+SO2	0.98010000	0.99970200	0.99942660			
	60	SO1+SO2	0.98010000	0.99970200	0.99942660			
	100	SO1+SO2	0.98010000	0.99962100	0.99942660			
0.950	20	SO1	0.99500625	0.99998128	0.99996013	0.99500625	0.99873470	0.99840783
	60	SO1	0.99500625	0.99938338	0.99916339			
	100	SO1	0.99500625	0.99873470	0.99840783			
	20	SO1+SO2	0.99500625	0.99998128	0.99996041			
	60	SO1+SO2	0.99500625	0.99998128	0.99996041			
	100	SO1+SO2	0.99500625	0.99997564	0.99996041			
0.990	20	SO1	0.99980001	0.99999997	0.99999993	0.99980001	0.99998918	0.99998626
	60	SO1	0.99980001	0.99999501	0.99999306			
	100	SO1	0.99980001	0.99998918	0.99998626			
	20	SO1+SO2	0.99980001	0.99999997	0.99999993			
	60	SO1+SO2	0.99980001	0.99999997	0.99999993			
	100	SO1+SO2	0.99980001	0.99999996	0.99999993			

SUMMARY AND CONCLUSION

This manuscript presents a description, analysis, example and reliability study for novel, redundant, radial and combination, homopolar magnetic bearings. Current distribution matrices (CDM) are evaluated based on the set of poles that have failed and the requirements for uncoupled force/voltage control, linearity and specified force/voltage gains that are unaffected by the failure. The CDM algorithm also determines the CDM with a minimum Frobenius norm which provides reduced effort (current required) operation of the HOMB. An advantage of the HOMB over a HEMB is the automatic invariance of the position stiffness before and after pole failure. This results from the bias flux source being permanent magnets. A simplified catcher bearing model is employed to evaluate the improvement in reliability which results from utilizing a success criterion (SO2) based on re-levitation after catcher bearing contact vs. a criterion (SO1) which excludes all contacts with the spinning shaft. The SO1 criterion is more conservative since it does not depend on the accuracy of the catcher bearing model used in the simulation.

The numerical example presented exhibits several interesting trends which include

- the reliability of the 4, 6 or 7 pole bearing is high even if the reliability of the pole decreases with time to 0.90.
- increased reliability with increased number of poles
- high reliability without replacing the no-poles failed CDM with the appropriate poles-failed CDM
- successful levitation with only 2 unfailed poles for the n = 4, 6 and 7 pole HOMB's
- successful fault tolerant operation without changes to the MIMO control in Fig. 18.

Future work includes tests of 6 pole radial and combination HOMB's in the G2-ACESE flywheel module at NASA Glenn. A higher fidelity catcher bearing model will also be employed in future simulations to provide a more realistic evaluation of the SO2 type reliabilities. Finally the MIMO control will also be modified to improve the reliability without replacing the no-poles failed CDM with a pole-failed CDM's.

NOMENCLATURE

a	=	radial pole face area of combo bearing
a'	=	axial pole face area of combo bearing
a_d	=	dead pole face area of radial bearing
B	=	flux density vector
B_{bias}	=	bias flux density vector
C_c	=	contact damping
C_e	=	housing damping
e	=	rotor eccentricity
$F_{(\ )}^A, F_{(\ )}^B$	=	force
g	=	acceleration of gravity
$g_{(\ )}$	=	air gap of the radial pole
g_{0d}	=	air gap of dead pole of radial bearing
H_c	=	coercive force of permanent magnet
$I_{(\ )}$	=	current
$I_{t(\ )}, I_{p(\ )}$	=	transverse and polar moment of inertia
$K_{p(\ )(\ )}$	=	position stiffness
$K_{V(\ )(\ )}$	=	control voltage stiffness
K_c	=	contact stiffness
K_e	=	housing stiffness
L_{pm}	=	length of permanent magnet
$L_{(\ )}^A, L_{(\ )}^B$	=	distance from the center of flywheel or housing coordinate
M_r	=	mass of rotor
M_h	=	mass of housing
$M_{(\ )}^A, M_{(\ )}^B$	=	moment
$N_{(\ )}$	=	number of turns of coils
N_{c1}, N_{c2}, N_{c3}	=	number of turns on decoupling chokes
R_i	=	reluctance of air gap
R_{pm}	=	reluctance of permanent magnet
R_{c1}, R_{c2}	=	air gap reluctance of decoupling chokes
$T_{(\ )}^A, T_{(\ )}^B$	=	current distribution matrix

Φ	=	flux vector
ω	=	rotor angular velocity
μ	=	dynamic friction coefficient
$\theta_{(\ )}$	=	angle of the radial pole

REFERENCES

[1]Iwaki, S., 1990, "The Optimal Location of Electromagnets in Multiple Degree of Freedom Magnetically Suspended Actuators," ASME J. Dynamic Systems, Measurement, and Control, 112, pp. 690-695.

[2]Meeker, D. C., 1996, "Optimal Solution to the Inverse Problem in Quadratic Magnetic Actuators," Ph.D. dissertation, University of Virginia.

[3]Maslen, E. H., and Meeker, D. C., 1995, "Fault Tolerance of Magnetic Bearings by Generalized Bias Current Linearization," IEEE Trans. Magn., 31(3), pp. 2304-2314.

[4]Maslen, E. H., Sortore, C. K., and Gillies, G. T., 1999, "Fault Tolerant Magnetic Bearings," ASME J. Engineering for Gas Turbines and Power, 121, pp. 504-508.

[5]Na, UJ, and Palazzolo, A., 2000, "Optimized Realization of Fault-Tolerant Heteropolar Magnetic Bearings," ASME J. Vibration and Acoustics, 122, pp. 209-221.

[6]Na, UJ, Palazzolo, A., and Provenza, Andrew, 2002, "Test and Theory Correlation Study for a Flexible Rotor on Fault-Tolerant Magnetic Bearings," ASME J. Vibration and Acoustics, 124, pp. 359-366.

[7]Na, UJ, and Palazzolo, A., 2000, "Fault Tolerance of Magnetic Bearings with Material Path Reluctances and Fringing Factors," IEEE Trans. Magn., 36(6), pp. 3939-3946.

[8]Maslen, E. H., Allaire, P. E., Noh, M. D., and Sortore, C. K., 1996, "Magnetic Bearing Design for Reduced Power Consumption," ASME J. Tribology, 118, pp. 839-846.

[9]Skogestad, S. and Postlethwaite, I., 1996, Multivariable Feedback Control, John Wiley & Sons, pp. 519.

[10]Sun, G., Palazzolo, A., and Kaushik, N., 2003, "An Efficient Algorithm for Blade Loss Simulations Using a High Fidelity Ball Bearing and Damper Model," ASME Design Engineering Technical Conferences and Computers and Information in Engineering Conference, Chicago, Illinois USA.

[11]Okada, Y., Nagai, B. and Shimane, T., 1992, "Cross Feedback Stabilization of the Digitally Controlled Magnetic Bearing," ASME J. Vibration and Acoustics, 114, pp. 54-59.

[12]Ahrens, M., Traxler, A., Von Burg, P., and Schweitzer, G., 1994, "Design of a Magnetically Suspended Flywheel Energy Storage Device," Fourth International Symposium on Magnetic Bearings, ETH Zurich, pp. 553-558.

[13]Ahrens, M., Kucera, L., and Larsonneur, R., 1996, "Performance of a Magnetically Suspended Flywheel Energy Storage Device," IEEE Trans. on Control System Technology, 4, pp. 494-502.

REPORT DOCUMENTATION PAGE

1. AGENCY USE ONLY (Leave blank)	2. REPORT DATE	3. REPORT TYPE AND DATES COVERED
	September 2003	Technical Memorandum

4. TITLE AND SUBTITLE

Fault Tolerant Homopolar Magnetic Bearings

5. FUNDING NUMBERS

WBS–22–755–60–12

6. AUTHOR(S)

Ming-hsiu Li, Alan Palazzolo, Andrew Kenny, Andrew Provenza, Raymond Beach, and Albert Kascak

7. PERFORMING ORGANIZATION NAME(S) AND ADDRESS(ES)

National Aeronautics and Space Administration
John H. Glenn Research Center at Lewis Field
Cleveland, Ohio 44135–3191

8. PERFORMING ORGANIZATION REPORT NUMBER

E–14149

9. SPONSORING/MONITORING AGENCY NAME(S) AND ADDRESS(ES)

National Aeronautics and Space Administration
Washington, DC 20546–0001

10. SPONSORING/MONITORING AGENCY REPORT NUMBER

NASA TM—2003-212592
AIAA–2003-6110

11. SUPPLEMENTARY NOTES

12a. DISTRIBUTION/AVAILABILITY STATEMENT

12b. DISTRIBUTION CODE

13. ABSTRACT (Maximum 200 words)

Magnetic suspensions (MS) satisfy the long life and low loss conditions demanded by satellite and ISS based flywheels used for Energy Storage and Attitude Control (ACESE) service. This paper summarizes the development of a novel MS that improves reliability via fault tolerant operation. Specifically, flux coupling between poles of a homopolar magnetic bearing is shown to deliver desired forces even after termination of coil currents to a subset of "failed poles." Linear, coordinate decoupled force-voltage relations are also maintained before and after failure by bias linearization. Current distribution matrices (CDM) which adjust the currents and fluxes following a pole set failure are determined for many faulted pole combinations. The CDM's and the system responses are obtained utilizing 1D magnetic circuit models with fringe and leakage factors derived from detailed, 3D, finite element field models. Reliability results are presented versus detection/correction delay time and individual power amplifier reliability for 4, 6, and 7 pole configurations. Reliability is shown for two "success" criteria, i.e. (a) no catcher bearing contact following pole failures and (b) re-levitation off of the catcher bearings following pole failures. An advantage of the method presented over other redundant operation approaches is a significantly reduced requirement for backup hardware such as additional actuators or power amplifiers.

14. SUBJECT TERMS

Magnetic bearing; Fault tolerant; Homopolar bearings

15. NUMBER OF PAGES

24

16. PRICE CODE

17. SECURITY CLASSIFICATION OF REPORT	18. SECURITY CLASSIFICATION OF THIS PAGE	19. SECURITY CLASSIFICATION OF ABSTRACT	20. LIMITATION OF ABSTRACT
Unclassified	Unclassified	Unclassified	